Electronics and Communications in Japan, Part 2, Vol. 70, No. 2, 1987
Translated from Denshi Tsushin Gakkai Ronbunshi, Vol. 69-C, No. 4, April 1986, pp. 421-432

1.5 μm InGaAsP Fabry-Perot Cavity-Type Laser Amplifiers

Takaaki Mukai, Tadashi Saitoh, and Osamu Mikami, Members

NTT Electrical Communications Laboratories, Musashino, Japan 180

SUMMARY

To understand the small-signal gain, signal-gain saturation and noise characteristics of 1.5 μm InGaAsP Fabry-Perot cavity-type laser amplifiers, two types of laser amplifiers having different thickness of the active layers were tested. It was found that the larger the gain coefficient (i.e., the larger the injected carrier density), the higher the gain and saturation output of the amplifiers, and the lower the noise level. Stern's gain calculation method was applied to materials for the 1.5-μm region. It was found theoretically that these characteristics are due to the dependence of the carrier lifetime on the injected carrier density and the dependence of the saturation intensity and the population inversion parameter of the gain coefficient, by using the material parameters taking account of the Auger effect and the structure parameters of the device. The feature of the 1.5-μm amplifiers is that the reduction of the carrier lifetime with the increase of the carrier density becomes more significant due to the Auger recombination process. It is important for improving the saturation output by positively utilizing this phenomenon to design the amplifier structure so that the amplifiers can be operated in a high-gain region.

1. Introduction

Semiconductor lasers which have been developed as small, highly efficient and long-lived oscillators operate as linear optical amplifiers which directly amplify an external optical signal when they are biased below the oscillation threshold [1, 2]. A small-signal gain, the signal gain saturation [3, 5], noises [2, 6, 7] which are fundamental characteristics of a Fabry-Perot (FP) type and traveling-wave-type optical amplifiers have been elucidated experimentally and theoretically by using 0.8-μm AlGaAs semiconductor laser amplifiers. By an experimental transmission of PCM-IM signal (100 M bits/s) using AlGaAs semiconductor laser amplifiers [13], it has been shown that this type of amplifier is used for an optical preamplifier [8, 9] set just in front of the photodetector, and the minimum receiving level can be improved compared with a conventional APD detector. It has also been demonstrated that it is possible to reduce the size of the repeaters and substantially expand the regenerative repeater spacing [11, 12] when this type of amplifier is used as optical linear repeaters [10]. For a further extension of applications of the optical amplifiers to optical transmission systems, it is essential to materialize an InGaAsP laser amplifier for a long-wavelength region in which optical fibers become low-loss and low-dispersion, and to optimize its device characteristics by their quantitative analyses.

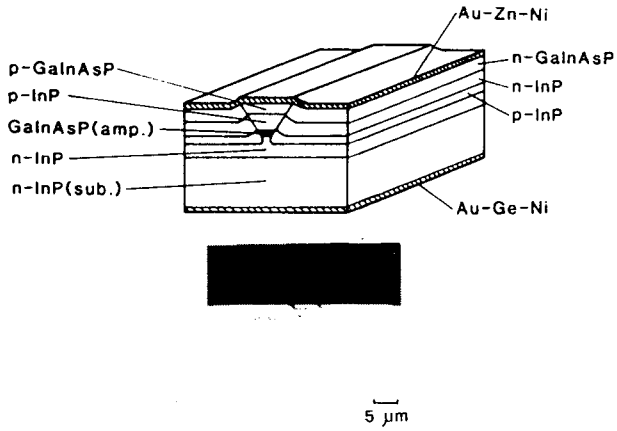

Fig. 1. Schematic drawing and SEM cross section for 1.5 μm BH laser amplifier.

ISSN8756-663X/87/0002-0038$7.50/0

Table 1. Device, structure parameters and material parameters of the InGaAsP amplifiers

Amplifier		a (○)	b (△)
Active layer		nondope	nondope
Device parameters			
Oscillation Wavelength	λ (μm)	1.504	1.536
Oscillation threshold	I_{th} (mA)	36.4	20.2
Gr. refractive index	n_g	3.53	3.8
Absorption coeff.	α (cm^{-1})	2 1	2 9
Thickness of active layer	d (μm)	0.09	0.17
Width of active layer	w (μm)	2.8	2.7
Length of cavity	L (μm)	190	290
Facet reflectivity	R (%)	30.4	35.2
Structure parameters			
Confinement factor	Γ	0.136	0.361
Optical model volume	$V_0(m^3)$	3.52×10^{-16}	3.69×10^{-16}
Photon lifetime	τ_p (ps)	1.4	1.95
Material parameters			
	A_g ($-dg/dN_e$) (m^2)	4.63×10^{-20}	
	N_0 (m^{-3})	8.3×10^{23}	
Carrier lifetime	τ_s (ns)	0.4	1.4

We fabricate 1.5 μm InGaAsP FP cavity-type laser amplifiers [14] using a buried heterostructure with different thickness of active layers. The dependence of their small-signal gain, signal gain saturation, and noise characteristic on the structure are studied experimentally in this paper. The amplifier having a thinner active layer and a smaller mode-confinement factor was found to have a higher signal gain, a higher saturation output, and a lower noise level. Furthermore, Stern's gain calculation method was applied to materials for the 1.5 μm region. Nonradiative recombination lifetime due to Auger effect is also taken into account for evaluating the carrier lifetime. Amplifier device characteristics were analyzed theoretically by using both the material parameters and the structure parameters relevant to each amplifier. The differences of the small signal gain, gain saturation and noise characteristic between amplifiers having different active layer thickness are attributed theoretically to the dependence of the carrier lifetime on the injected-carrier density, and the dependence of the saturation intensity and the population-inversion parameter on the gain coefficient, respectively. The feature of the 1.5-μm amplifier is the rapid reduction of the carrier lifetime with the increase of the carrier density due to the Auger recombination process. Finally, the importance of designing the amplifier should be pointed out: it should be capable of operating in a high-gain region where this phenomenon contributes to high-saturation output and high signal gain.

2. Structure Parameters and Material Parameters of the 1.5-μm Laser Amplifiers

2.1 Fabrication of the InGaAsP amplifiers and their structure parameters

Figure 1 shows the schematic drawing of the 1.5-μm InGaAsP buried heterostructure (BH) laser amplifier, and its sectional view obtained by the SEM observation. The device was fabricated by using the low-temperature liquid-phase epitaxial growth [15], as follows. In the first growth, the *n*-InP layer (Sn doped), InGaAsP active layer (nondoped),

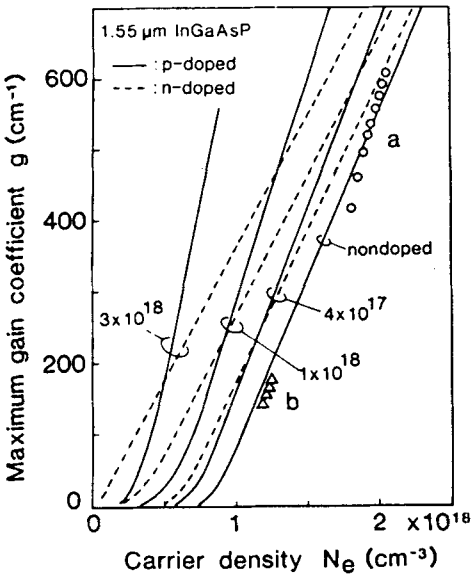

Fig. 2. Theoretical and experimental peak gain coefficient g vs. the minority carrier density N_e for 1.55-μm InGaAsP lasers.

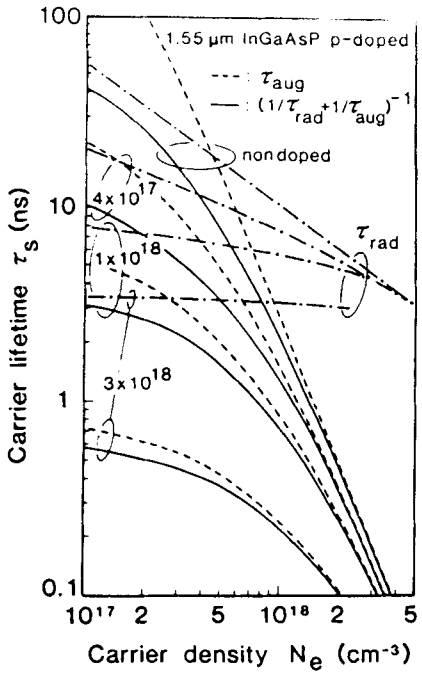

Fig. 3. Carrier lifetime τ_s vs. the minority carrier density N_e for p-doped 1.55-μm InGaAsP lasers.

p-InP layer (Zn doped), and p-InGaAsP cap layer (Zn doped) were successively grown on the (001) oriented n-InP substrate so that a double heterostructure was formed. Then an SiO_2 film pattern having a width of 8 μm in the <110> direction was formed by using the RF sputtering method and the photolithography method. This was etched with bromine-methanol solution so that a mesa structure having an active layer about 2.8 μm wide was formed. In the second growth, a p-InP layer, n-InP layer and n-InGaAsP layer were successively grown. The leakage of the injection current outside the active layer is prevented by the reversed biased p-n junction in the burying region.

Au-Zn-Ni is vacuum-evaporated and amalgamed for the p-electrode, and Au-Ge-Ni for the n-electrode. Then chips 200 to 300 μm long were made by cleaving. The chip was mounted on a diamond heat sink with In solder. The threshold value of the BH laser fabricated is between 20 and 36 mA. The lasers operated in a single longitudinal mode with about 1.6 times the threshold value.

Two kinds of BH amplifier (a and b) having the thickness of the active layer of 0.09 and 0.17 μm, respectively, were used in the experiment for studying the structure dependence of the optical amplifier characteristics in the 1.5-μm region. Table 1 shows the structure parameters and the material parameters of the two kinds of amplifier.

The absorption coefficient α is obtained from the dependence of the external differential quantum efficiency on the cavity length of the lasers which were taken from the same wafer used. The group refractive index n_g was obtained by measuring the longitudinal-mode spacing frequency in the gain spectrum. The optical-mode confinement factor Γ for the active layer [16], and the facet reflectivity R for the TE polarized wave of the cleaved facet [17] were obtained from the slab waveguide analysis, by using the refractive indices $n_{act} = 3.523$ [18] and $n_{clad} = 3.17$. By using these values, important structure parameters of the amplifier, such as the mode confinement factor Γ, the optical mode volume V_0 ($=dwL/\Gamma$, where w is the width of the active layer), and the photon lifetime τ_p ($=[v_g\{\alpha+(1/L)\ln(1/R)\}]^{-1}$, $v_g = c/n_g$, which is the group velocity in the medium) were derived.

2.2 Material parameters of the InGaAsP amplifier

The gain spectra of $In_{0.58}Ga_{0.42}As_{0.9}P_{0.1}$ for the band-gap wavelength of

1.55 μm were calculated as a function of injected carrier density by using the density of states with the Kane function interpolated to the Halperin-Lax bandtail and Stern's improved matrix element [19, 20]. This was done by applying the equation, which Dutta used for the 1.3 μm InGaAsP material [21], to $y = 0.9$ for the band structure parameters of the material for 1.55 μm, with the values of $E_g = 0.8$ eV, $m_c/m_0 = 0.045$, $m_{hh}/m_0 = 0.44$, $m_{lh}/m_0 = 0.057$, $\varepsilon = 12.2$ and $\Delta = 0.32$ eV.

Figure 2 shows the dependence of the peak gain coefficient g (obtained from the calculation of the gain spectrum) on the injected carrier density N_e, with various concentrations of the doping materials. From these, the relationships between g and N_e are given by

$$g = A_g(N_e - N_0) \tag{1}$$

where A_g(m^2) is the slope of the gain coefficient vs. injected carrier density curve, and N_0 is the density of the minority carriers which makes the stimulated emission greater than the stimulated absorption. In the case of a p-doped material, N_0 reduces and A_g increases with the increase of the dopant concentration. In the case of n-doped material, both N_0 and A_g reduce. The experimental values shown in Fig. 2 were obtained by the gain measurements described later. These show that the amplifier a works in a region where the injected carrier density and the gain coefficient are greater than those of b.

Figure 3 shows the dependence of the carrier lifetime τ_s on the injected carrier density, for various p-dopant concentrations; τ_s (shown by solid lines in Fig. 3) is represented by the resultant of the lifetime due to the radiative recombination process τ_{rad} and the lifetime due to the nonradiative recombination process τ_{nr}, i.e.,

$$1/\tau_s = 1/\tau_{rad} + 1/\tau_{nr} \tag{2}$$

τ_{rad} (shown by dash-dotted lines) is obtained as a function of N_e by integrating spontaneous emission power in a thermal equilibrium condition (which is obtained in the above-described gain spectrum calculation) [19]. Since the dominant nonradiative recombination process in the 1.5-μm material is the Auger recombination of the CHSH

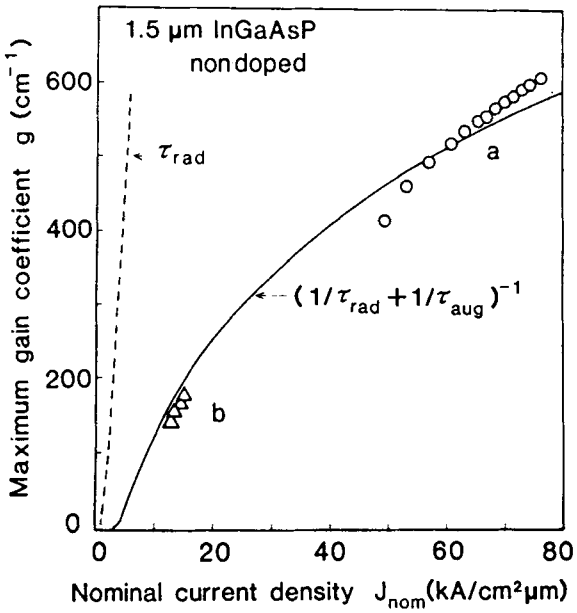

Fig. 4. Theoretical and experimental peak gain coefficient g vs. the nominal current density J_{nom} for nondoped 1.55 μm InGaAsP lasers.

process [22], the Auger lifetime τ_{aug} [23] is used for τ_{nr}; τ_{aug} is shown by dashed lines in Fig. 3; τ_s decreases rapidly with N_e, since the recombination rate is proportional to the cube of the injected carrier density in the Auger recombination, unlike that in a material having a small concentration of impurity in which the recombination rate is proportional to the square of the injected carrier density. This effect is seen in the dependence of the gain coefficient on the nominal current density J_{nom} $(=eN_e/\tau_s(N_e))$.

Figure 4 shows the $g - J_{nom}$ curves of nondoped InGaAsP obtained from $g(N_e)$ and $\tau_s(N_e)$ in Figs. 2 and 3. The value of g consisting of $\tau_{rad}(N_e)$ alone increases linearly with J_{nom} (shown by a dashed line). By contrast, the value of g including τ_{aug} (shown by a solid line) tends to saturate, due to the rapid decrease of τ_{aug}. The experimental values of a and b (shown by circles and triangles in Fig. 3) were obtained from the signal gain measured by the optical injection method (described later in Fig. 5). These

values have a good agreement with the solid curve in Fig. 4.

Table 1 also tabulates the theoretical values of the material parameters; A_g $(=dg/dN_e)$, N_0 and the carrier lifetime τ_s at the threshold of the amplifiers a and b used for the experiment, which significantly affect their amplification characteristics.

3. Signal Gain and Saturation

3.1 Small-signal gain

The signal gain G of an FP cavity-type optical amplifier for a small-signal optical input having a frequency f is given by

$$G(f)=\frac{(1-R)^2 G_s}{(1-RG_s)^2+4RG_s\sin^2[2\pi(f-f_0)L/v_g]} \tag{3}$$

where G_s is the single-pass gain. This is related with the gain coefficient g by

$$G_s=\exp[(\Gamma g-\alpha)L] \tag{4}$$

The ratio v of the output of the amplified signals in a resonant state ($f = f_0$) and a nonresonant state ($f = f_0 + v_g/4L$) is given by

$$v=\frac{G(f_0)}{G(f_0+v_g/4L)}=\left(\frac{1+RG_s}{1-RG_s}\right)^2 \tag{5}$$

By measuring the value of v, G_s is given by

$$G_s=\frac{1}{R}\cdot\frac{\sqrt{v}-1}{\sqrt{v}+1} \tag{6}$$

Therefore, G is given from Eq. (3), and g is given from Eq. (4).

From Eq. (3), the gain profile of the single-longitudinal mode in the small-signal region is given for $f-f_0 \ll (v_g/2L)$ by the following Lorentz-type equation:

$$\frac{G(f)}{G(f_0)}=\frac{1}{1+[(f-f_0)/B]^2} \tag{7}$$

where B is the half-width at half-maximum (HWHM) of the signal gain profile given by

$$B=(v_g/2\pi L)\sin^{-1}[(1-R)/2\sqrt{RG(f_0)}] \tag{8}$$

This shows that $\sqrt{G}B$ becomes constant in each amplifier. By measuring B, therefore, the signal G can be obtained from Eq. (8).

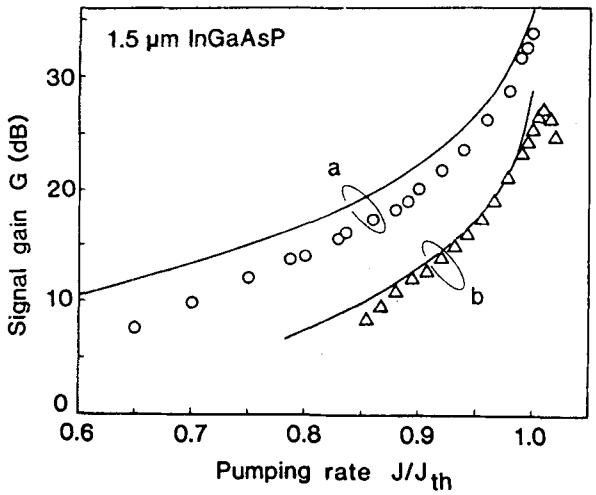

Fig. 5. Unsaturated signal gain G for TE input signal light vs. the amplifier pumping rate J/J_{th}.

It has been confirmed that the two types of measuring methods using Eqs. (6) and (8), respectively, give the same results in the experiment, using the 0.8 μm AlGaAs amplifier [3]. The gain measuring method using the value of v (Eq. (6)) however, has a poor accuracy for the InGaAsP amplifier, since InP used for the cladding layer is transparent to the optical input signal of 1.5 μm so that most input optical power passes through the cladding layer without coupling into the amplifier waveguide. Therefore, we used the optical injection method [1-3] with the measurement of the HWHM bandwidth B (Eq. (8)) to obtain the signal gain. The $\sqrt{G}B$ of the amplifier a and b used are 45 and 24 GHz, respectively.

The experiment was carried out by using the same arrangement as shown in [3, Fig. 1]. In this experiment, the output of an InGaAsP laser which produces a single longitudinal-mode oscillation is coupled into the optical amplifier through an optical isolator and an optical chopper. The amplified output power is detected using a lock-in amplifier so that the influence of the spontaneous emission is eliminated. The temperatures of the amplifier and the oscillator were controlled to within 0.01°C by using a Peltier element. Frequency tuning between the amplifier FP mode and the input signal is achieved by controlling mainly the temperature of the amplifier. The bandwidth B which determines the signal gain was obtained from the temperature change of the amplifier.

Figure 5 shows the dependence of the small-signal gain in a resonant state on the normalized pumping rate for the TE polarized input signal. The signal gain increases with the pumping rate and becomes between 27 and 33 dB at the lasing threshold. The solid lines in Fig. 5 were obtained theoretically by using the $g - J_{nom}$ curve (Fig. 4) and Eqs. (3) and (4). A larger signal-gain is obtained by the amplifier a which has a smaller value of Γ than the amplifier b, with the same normalized pumping rate. In the amplifier a, the rate of the signal gain change against the pumping rate change is more decreased than in the amplifier b. This is due to the operation of amplifier a in a region where the change of the gain coefficient against the injection current is reduced. This reduction is caused by the reduction of the carrier lifetime due to the Auger recombination in the region where the injection current is large.

3.2 Gain saturation and saturation intensity

Figure 6 shows the dependence of the tuning characteristic of the amplified output signal on the optical input signal power, obtained by feeding the optical output of the laser oscillator into the optical amplifier b, and by sweeping the temperature of the amplifier. When the optical input power is small, the gain profile is the Lorentz-type represented by Eq. (7). When the optical input power is increased, the peak wavelength of the signal gain shifts towards a longer wavelength, and the profile becomes asymmetrical. As is already reported for a GaAs amplifier [5], this is due to the increase of the refractive index of the active layer owing to the reduction of the rejected carrier density stemming from the gain saturation, resulting from the increase of the resonance frequency of the amplifier.

The inset in Fig. 7 shows the block diagram used for measuring the saturated signal gain. This method was used because the gain profiles in the gain-saturated region do not follow Eq. (7), i.e., the signal gain measuring method by using the bandwidth B cannot be applied. By using the same Ge photodiode (PD) having a large diameter, the optical output vs. injection current characteristics were measured behind a half-mirror P_4 and at the amplifier output facet P_3. Then the output coupling efficiency η was obtained from the ratio of the external differential quantum efficiency above the threshold value. Figure 7 shows experimental results for P_3 and P_2 as a function of the optical input

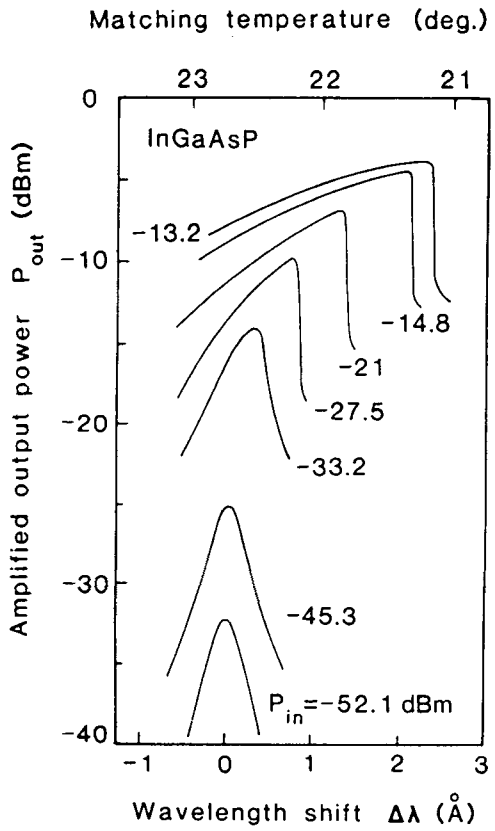

Fig. 6. Amplifier gain profiles are changed due to gain saturation. Resonance condition is met at longer wavelength and gain profile becomes more asymmetric with the increase of the input power (sample b).

power P_1 measured at the immediate front of the input coupling lens. The output power P_3 was derived by $P_3 = P_4/\eta$, where P_4 is the power actually measured. P_2 is the input power derived by $P_2 = P_3/G$, where G is the signal gain obtained by using Eq. (8). The values of P_2 show a good agreement with the broken line (in Fig. 7) having a declination of 1 (corresponding to the input coupling loss of 6 dB), notably in a small-signal gain region below P_1 = -30 dBm. This ensures that the experiment was carried out with a constant coupling efficiency. The amounts of P_3 increased from the broken line of P_2 are plotted in Fig. 8 as the signal gain including the saturation region.

Figure 8 shows the dependence of the signal gain at a resonant state of the amplifiers a and b on the amplified output power with unsaturated signal gains of 20 and

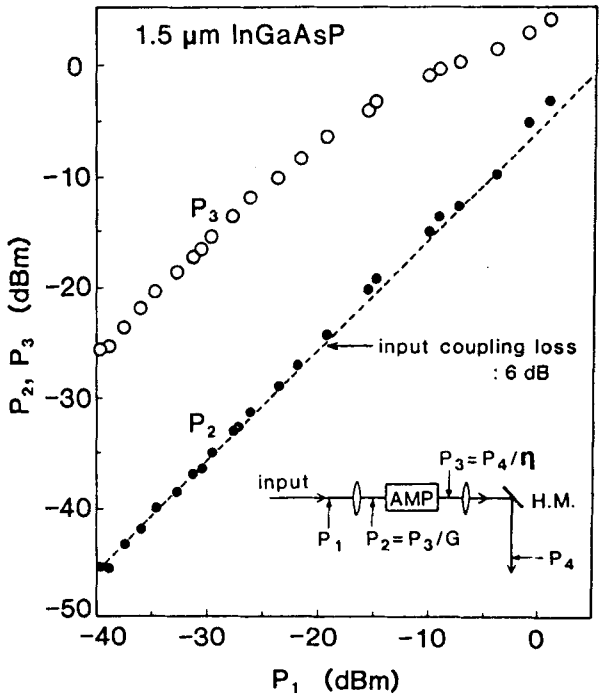

Fig. 7. Signal gain in the saturation region is measured as the ratio of P_3 to the dashed line of P_2 (sample a).

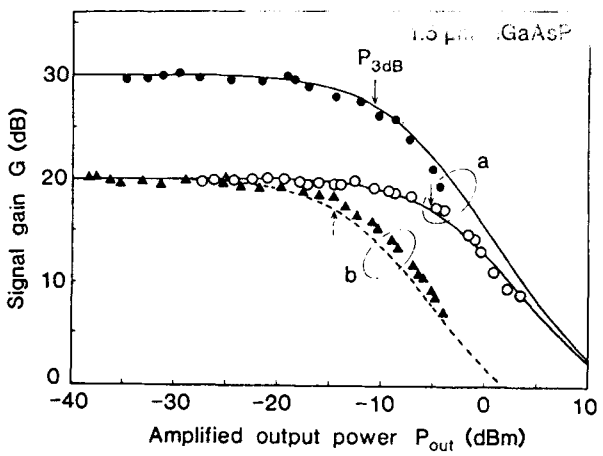

Fig. 8. Theoretical and experimental signal gain at resonance condition vs. the amplified output power.

30 dB. When the output power increases, the signal gain decreases due to the gain saturation. Let us define "the saturation output power P_{3dB}" as the output at which signal gain is reduced by 3 dB from the unsaturated value. P_{3dB} reduces with the increase of the unsaturated signal gain. P_{3dB} at the unsaturated signal gain of 20 dB is -4.8 dBm for the amplifier a, and -13.5 dBm for the amplifier b, the former being improved greatly. This difference is attributed to the differences of the structure parameters and the material parameters of the two amplifiers.

The gain saturation of an optical amplifier is caused by the reduction of the population inversion in the active layer due to the increase of the stimulated emission. The injected carrier density can be determined by using the following single-mode rate equation [24] to which a term of the optical injection is added:

$$\frac{dN_c}{dt}=P-\frac{N_c}{\tau_s}-A\Gamma\left(\frac{N_c}{V_e}-N_0\right)n \qquad (9)$$

$$\frac{dn}{dt}=-\frac{n}{\tau_p}+\frac{A\Gamma N_c}{V_e}+A\Gamma\left(\frac{N_c}{V_e}-N_0\right)n+P_{in} \qquad (10)$$

where N_c is the number of the injected carriers ($=N_e \cdot V_e$) in the volume of the active layer V_e ($=\Gamma V_0$); n is the number of the photons in the fundamental mode; P is the pumping rate; P_{in} is the number of the injected signal photons and A ($=A_g \cdot V_g$) is the differential gain coefficient per unit time with respect to the carrier density (m^3/s). The solid lines and broken line in Fig. 8 are the theoretical results obtained from the numerical calculations by using Eqs. (3), (4), (9) and (10) in conjunction with structure parameters and the material parameters of the two amplifiers, respectively.

To understand the physical meaning of the gain saturation, it is important to examine the following equation obtained by substituting the steady-state solution of N_c [derived from Eq. (9)] into Eq. (1):

$$g=\frac{g_0}{1+\beta n} \qquad (11)$$

where g_0 is the unsaturated gain coefficient for a case where the number of the injected carriers for the pumping is determined by the spontaneous emission alone, without any stimulated emission (n = 0); β is the spontaneous emission coefficient which is given from the second term of Eq. (10) [24, 25] by

$$\beta=A\tau_s/V_0 \qquad (12)$$

Equation (11) shows that the gain coefficient g reduces with the increase of the number of photons in the cavity n; g is $g_0/2$ when n is

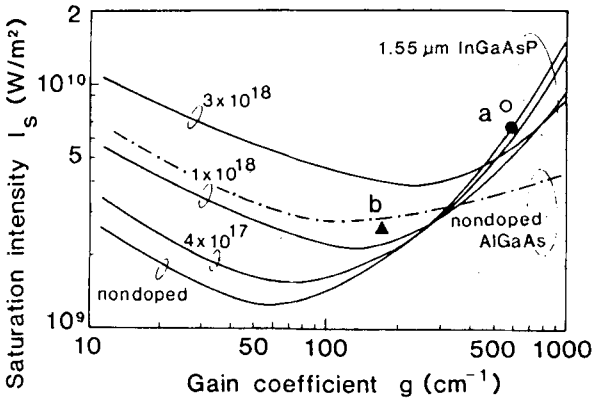

Fig. 9. Theoretical and experimental saturation intensity I_s vs. the gain coefficient g for p-doped 1.55 μm InGaAsP lasers.

$1/\beta$. An amplifier having a smaller β, therefore, has a larger saturation output. From Eq. (12), the theoretical values β of the amplifiers a and b are given by 4.5×10^{-6} and 1.4×10^{-5}, respectively.

By representing the number of the photons in the active layer by the optical intensity I ($=hfv_g n/V_0$), the following equation is obtained:

$$g=\frac{g_0}{1+I/I_s} \tag{13}$$

where I_s(W/m^2) is the saturation intensity [26, 3] defined by the optical intensity which reduces g to $g_0/2$; I_s is given by

$$I_s=\frac{hfv_g}{A\tau_s}=\left(\frac{hfv_g}{V_0}\right)\frac{1}{\beta} \tag{14}$$

Figure 9 shows the dependence of I_s on the gain coefficient with different concentrations of the p-type dopant; I_s is determined by the material parameters of the amplifier A_g ($=A/v_g$); τ_s and the photon energy hf. A large value of I_s in the region of a small g is due to the fact that A_g becomes smaller at the raised part of the gain coefficient (see Fig. 2). The increase of I_s in the region of a large g is due to the fact that τ_s reduces with the carrier density (see Fig. 3). In general, as the dopant concentration is increased, I_s becomes greater in a region where g is wider due to shortened τ_s value.

I_s is smaller in the region where g is smaller, since the photon energy in the InGaAsP amplifier is about half compared with the AlGaAs amplifier having a nondoped active layer (shown by a dash-dotted line in Fig. 9); I_s is larger in a region where g is larger, since the reduction of τ_s is significant due to the Auger recombination. The I_s obtained from the experimental value of P_{3dB} (in Fig. 8) are also shown by a triangle and circles in Fig. 9; P_{3dB} for the amplifier a is larger than that for the amplifier b, since the former is operated with a larger I_s.

As shown in the forementioned examples, it is important for improving the saturation output of the 1.5-μm amplifier to design its structure so that the amplifier is operated in a region where g is large, and since the I_s dependence on the gain coefficient is more significant than the AlGaAs amplifier. To increase g, the reductions of the cavity length L, the mode confinement factor Γ, and the facet reflectivity R are effective [27]. To improve P_{out}/I, the increase of the mode sectional area V_0/L is desirable [3].

4. Noise Characteristics

When the output from an optical amplifier is detected by an avalanche-photodiode (APD), the noise power measured with the RF spectrum analyzer $P_m(\omega)$ is given [6] by

$$\begin{aligned}P_m(\omega)=&(2e^2\sigma^2_{beat}\eta^2\langle M\rangle^2+2e\langle i_{ph0}\rangle\\&\eta\langle M\rangle^{2+x})R_L B_0 G_e(\omega)\\&+P_{thermal}(\omega)\end{aligned} \tag{15}$$

where σ^2_{beat} is the variance value of the photon number per second corresponding to the beat noise component at the output terminal of the amplifier; $\langle M\rangle$ is the multiplication factor of the APD; x is the excess noise exponent of the APD; η is the product of the coupling efficiency (between the amplifier output and the APD) and the quantum efficiency; $\langle i_{ph0}\rangle$ is the photocurrent when the amplifier output is detected with $\eta = 1$ and $\langle M\rangle = 1$; e is the electron charge; R_L is the load resistance; B_0 is the resolution bandwidth of the spectrum analyzer; $G_e(\omega)$ is the overall frequency response of the APD and electronic amplifier circuits; and $P_{thermal}(\omega)$ is the thermal noise in the measurement equipment.

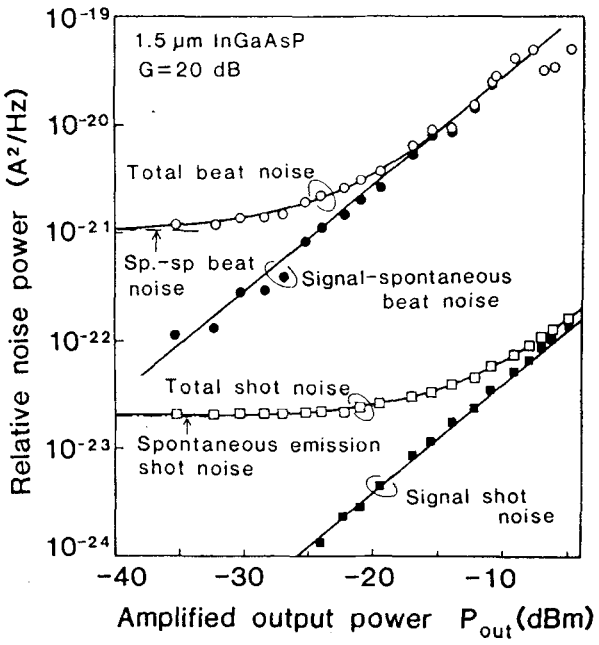

Fig. 10. Amplifier noise vs. the amplified output power (sample a).

The noise spectrum density per unit frequency (A^2/Hz) per unit of load resistance for the optical amplifier output is given by

$$\langle i_n^2 \rangle / B_0 = 2e^2 \sigma_{beat}^2 + 2e\langle i_{ph0} \rangle \qquad (16)$$

By using Eq. (15),

$$\frac{\langle i_n^2 \rangle}{B_0} = \frac{P_m(\omega) - P_{thermal}(\omega)}{R_L B_0 G_e(\omega) \eta^2 \langle M \rangle^2} + 2e\langle i_{ph0} \rangle \left(1 - \frac{\langle M \rangle^x}{\eta}\right) \qquad (17)$$

The first and second terms in Eq. (15) represent the beat-noise component and the shot noise component, respectively. The shot noise increases with a rate of the power of $(2 + x)$ of the APD multiplication factor $\langle M \rangle$, and the beat noise with a rate of the square of it. The whole efficiency η reduces proportionally to η in the shot noise, while η reduces at the rate of square of η in the beat noise. In this experiment, a $p^+ - n$ type Ge-APD [28] having $x = 0.83$ was used with η = -9 to -4 dB.

Figure 10 shows the dependence of the noise spectrum density of the amplifier *a* (signal gain 20 dB) on the amplified output signal P_{out}. The total noise is the sum of the beat noise between spontaneous emission components, the beat noise between the signal-spontaneous emission, the spontaneous emission shot noise, and the amplified signal shot noise. When the input optical signal level is less than -45 dBm, dominant amplifier noise is the beat noise between spontaneous emission components. The beat noise between the signal and spontaneous emission becomes dominant above this input signal level [6]. Among these two types of beat noise, the signal-spontaneous beat noise is inevitable in the optical amplifier, since this arises from the beat between the amplified optical signal and the spontaneous emission in the longitudinal mode related to the signal amplification. The spontaneous-spontaneous beat noise which occurs between the spontaneous emission components in all the longitudinal modes in the gain bandwidth, can be reduced by selecting the amplified longitudinal mode alone with the optical frequency filter.

The spectra of the two types of beat noise are free from resonance peak when they are below the threshold value [6]. The amplifier noise in the low-frequency region (order of few 100 MHz) can be given from the theoretical analysis [11, 13] (in which the master equation of the probability density function of the number of photons [29] are extended to the FP type amplifier) by

$$\sigma_{out}^2 = G\langle n_{in} \rangle + (G-1) n_{sp} m_t \Delta f_1 + 2G(G-1) n_{sp} \chi \langle n_{in} \rangle + (G-1)^2 n_{sp}^2 m_t \Delta f_2 \qquad (18)$$

where $\langle n_{in} \rangle$ is the number of photons incident on the amplifier, per second σ_{out}^2 is the variance value of the number of photons at the output, n_{sp} is the population inversion parameter of the amplification medium, χ is the excess noise coefficient for the signal-spontaneous beat noise, Δf_1 and Δf_2 are the equivalent noise bandwidths for the spontaneous emission shot noise and the spontaneous-spontaneous beat noise, respectively, and m_t is the effective degree of the transversal mode of the spontaneous emission [13].

From the first to the fourth term in Eq. (18) represents the amplified signal shot noise, the spontaneous emission shot noise, the signal-spontaneous beat noise, and the spontaneous-spontaneous beat noise. When $G = 1$, only the first term remains, representing a conventional signal shot noise. As Eq. (18) shows, the beat noise is greater than the shot noise by about G times.

From the traveling-wave type equation which is transformed from the rate equation of the number of photons in Eq. (10), the

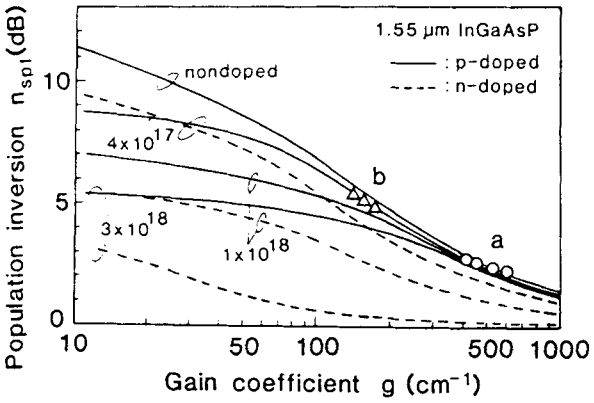

Fig. 11. Theoretical and experimental population inversion parameter n_{sp1} vs. the gain coefficient g.

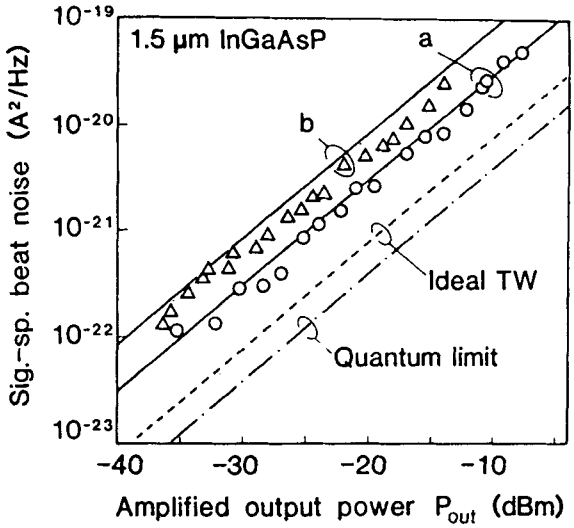

Fig. 12. Theoretical and experimental signal-spontaneous beat noise vs. the amplifier output power.

population inversion parameter n_{sp} is given by

$$n_{sp} = \frac{A\Gamma N_e}{A\Gamma(N_e - N_0) - \alpha v_g} = \frac{N_e}{N_e - N_0} \cdot \frac{\Gamma g}{\Gamma g - \alpha} \equiv n_{sp1} \cdot n_{sp2} \tag{19}$$

As Eq. (19) shows, the population inversion parameter is the result of two components n_{sp1} and n_{sp2}; n_{sp1} represents the degree of the ineffectiveness of the injected carrier density N_e for the stimulated emission which produces the net gain, because there is the carrier density N_0 corresponding to the stimulated absorption; n_{sp2} represents the contribution of the inner losses such as the free carrier absorption and the scattering loss. When n_{sp} approaches unity more ideal noise characteristics are obtained. Figure 11 shows n_{sp1} dependence on the gain-coefficient with various dopant concentration. Figure 11 also shows n_{sp1} of the amplifiers a and b obtained from the experimental values in Fig. 2. It is important for making n_{sp1} small to use an n-type active layer having a large dopant concentration, or to design the structure so that the amplifier works in a region where g is large; i.e., the reductions of Γ, L and R. By using Eqs. (4) and (6), n_{sp2} is represented by

$$n_{sp2} = 1 + (\alpha L) \cdot \left[\ln \frac{1}{R} \cdot \frac{\sqrt{v} - 1}{\sqrt{v} + 1} \right]^{-1} \tag{20}$$

This shows that n_{sp2} is reduced by reducing α, L and R.

The excess noise coefficient χ, which represents the increase of the signal-spontaneous beat noise caused by the reflectivity R_1 at the input terminal, is given [13] by

$$\chi = \frac{(1 + R_1 G_s)(G_s - 1)}{(1 - R_1) G_s} \tag{21}$$

χ approaches unity at an extreme with $R_1 = 0$ and $G_s \gg 1$ [27].

The equivalent noise bandwidth Δf_1 is obtained by summing the number of the spontaneously emitted photons in all the longitudinal modes; Δf_2 is obtained by summing the beat components in all the longitudinal mode which consists of the overlap integral of the number of spontaneously emitted photons in each longitudinal mode [11, 13]. For the calculation, an approximated equation $\Delta\lambda_g$ (Å) = 340 + 2.95 g (cm^{-1}) was used, where $\Delta\lambda_g$ is the wavelength full width for the positive gain coefficient of 1.5 μm nondoped InGaAsP material used for the experiment. This equation was obtained by calculating the gain shown in section 2.2.

Figure 12 shows the dependence of the signal-spontaneous beat noise (at the signal

Table 2. Noise figure of InGaAsP amplifiers (signal gain 20 dB)

Amplifier		a (○)	b (△)
Popu. invers. param.	n_{sp1}	2.2 dB	5.1 dB
	n_{sp2}	1.4 dB	2.8 dB
Excess noise coef.	χ	2.5 dB	2.5 dB
Noise fig. (Theor. val.)	F	9.1 dB	13.4 dB
Noise fig. (Meas. val.)	F	8.6 dB	11.5 dB

Noise fig. : $F = 2\, n_{sp1}\, n_{sp2}\, \chi$.

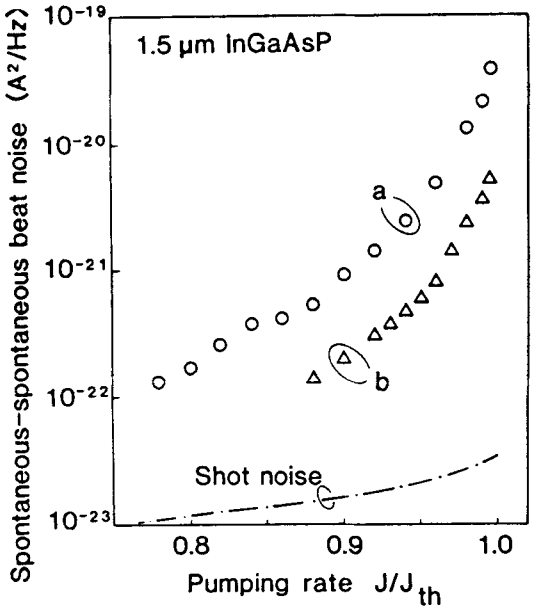

Fig. 13. Spontaneous-spontaneous beat noise dependence on the pumping rate.

gain of 20 dB) on the amplified output signal. The dash-dotted line shows the quantum limit obtained when a coherent optical signal having the level of $G\,P_{out}$ was received by an ideal detector (no thermal noise, and quantum efficiency 1). This level gives the same S/N value before and after the amplification. The increased amount from this value is the noise figure F [30] of the optical amplifier which is given by

$$F = 2 n_{sp} \chi \qquad (22)$$

The broken line shows the value of the signal-spontaneous beat noise obtained by an

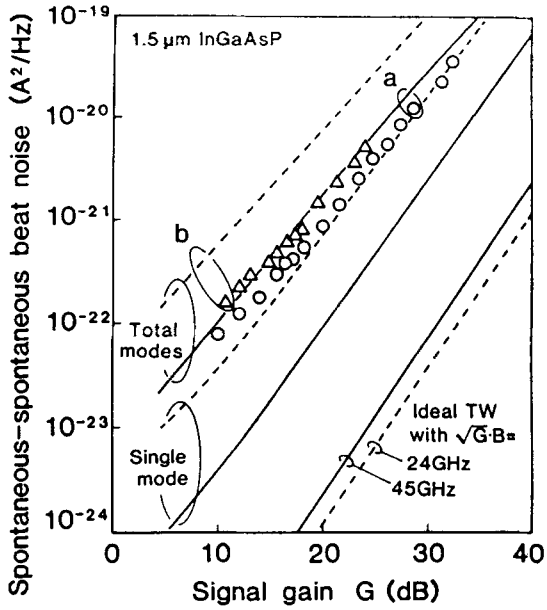

Fig. 14. Theoretical and experimental spontaneous-spontaneous beat noise vs. the signal gain G.

ideal traveling-wave amplifier having $n_{sp}\chi = 1$, the noise figure being 3 dB [31]. Table 2 shows the noise parameters of the FP cavity-type amplifiers a and b used in the experiment; i.e., n_{sp1}, n_{sp2}, χ and F. The noise figure for the amplifier a is smaller than that for b. This is due to the fact that the former is operated in a region where the gain coefficient is larger, and n_{sp} is smaller (see Fig. 11).

Figure 13 shows the dependence of the beat noise between spontaneous emission components on the normalized pumping rate. The spontaneous-spontaneous beat noise is greater than the spontaneous emission shot noise (shown by a dash-dotted line), and rapidly increases with the normalized pumping rate, the maximum value being around the threshold value [6]. The spontaneous-spontaneous beat noise is proportional to $(G-1)^2$ as shown by the fourth term of Eq. (18). The difference between the amplifiers a and b is attributed to the difference of the small-signal gain dependence on the pumping rate.

Figure 14 shows the dependence of the spontaneous-spontaneous beat noise on the small-signal gain. The spontaneous-spontaneous beat noise increases with the power of 1.1 to 1.2 (not 2) of the signal gain G. This is due to the fact that n_{sp}, Δf_2 and m_t

are reducing functions with respect to G. If only a single longitudinal mode which amplifies an input signal is selected using an optical frequency filter, the beat noise can be expected to reduce by about 10 dB. If an ideal traveling-wave amplifier having $n_{sp}\chi = 1$ and $m_t = 1$ is used, with an optical frequency filter having the $\sqrt{G}B$ characteristic (the same as the active-FP type filter), the noise would be reduced further by about 15 dB.

5. Guide for Designing the 1.5 μm-FP Cavity-Type Optical Amplifier

The relationship between the device characteristics and the material parameters and the structure parameters of the 1.5 μm optical amplifier, which was analyzed experimentally and theoretically in the foregoing sections, is summarized as follows.

For obtaining a large signal gain, it is necessary to increase the saturation output, as well as relaxing the small-signal gain dependence on the pumping rate. Since the latter is determined by the dependence of the gain coefficient on the nominal current density (see Fig. 4), it is necessary to operate the amplifier in a region where the carrier lifetime τ_s decreases rapidly with the increase of the carrier density, i.e., a region where the gain coefficient is large. Since the saturation output is determined by the saturation intensity I_s in Eq. (14), it is important to design the structure of the amplifier so that it is operated in a region where τ_s reduces rapidly with the increase of the carrier density, as well as to choose the active layer having small A_g and τ_s which determine the I_s (see Fig. 9).

The magnitude of the signal-spontaneous beat noise which is the substantial noise in an optical amplifier is determined by $n_{sp1} \cdot n_{sp2} \cdot \chi$. The reduction of the noise can be achieved, therefore, by operating the amplifier in a region where the injected carrier density N_e is large so that n_{sp1} is reduced by reducing the effect of N_0 relatively (see Fig. 11), and reducing n_{sp2} by reducing α, L and R. For reducing χ, the reduction of R_1 is necessary.

The forementioned analyses show that improvements of the device characteristics of the optical amplifier can be summarized in the following two points:

(1) use an active layer having the small values of A_g, N_0 and τ_s;

(2) design the structure of the amplifier so that it is operated with a larger gain coefficient and a larger injected carrier-density.

Thus it is desirable to use an active layer (notably n-type) having a high doping concentration for (1); and to reduce the length of the amplifier, the mode confinement Γ, and the facet reflectivity R for (2).

In the case of a laser oscillator, it is important for obtaining a large optical output to reduce the oscillation threshold value as much as possible. On the other hand, both the forementioned conditions for the optical amplifier which is operated below the oscillation threshold show the necessity of increasing the threshold value and setting the working point of the amplifier in a region where the injected carrier density N_e and the gain coefficient g are large.

The characteristic of the amplifier is not improved infinitely with the increase of the threshold value in terms of the structure design, but it is limited by the thermal saturation of gain, since the temperature rise due to the increase of the injection current reduces the gain coefficient (not mentioned previously). To minimize this limitation, it is important to improve the thermal characteristic [as a preparation of applying the condition (2)] by using the buried heterostructure which ensures carrier confinement.

The feature of the 1.5-μm InGaAsP amplifier is that the dependence of the carrier lifetime on the carrier density becomes more significant, compared with that of the AlGaAs amplifier, due to the Auger recombination process. To obtain the high saturation output in the InGaAsP amplifier, condition (2) [the realization of the operation in a small τ_s region] is more important than in the AlGaAs amplifier.

6. Conclusions

The 1.5 μm InGaAsP laser amplifiers having different active layer thickness were fabricated. The fundamental characteristics of the amplifiers, such as the small-signal gain, the gain saturation, and the noise, were analyzed quantitatively based on the material parameters of the semiconductor amplifying medium and the structure

parameters of the device. This shows that the amplifier which is operated with a larger carrier density has a higher gain, higher saturation output, and lower noise. It was explained theoretically that these improvements in the characteristics are due to the dependence of the carrier lifetime on the injected carrier density, and the dependences of the saturation intensity and the population inversion parameter on the gain coefficient.

The design policies relating to the material parameters and the structure parameters, which improve the device characteristics of the semiconductor optical amplifier, were discussed. It is indispensible for achieving the 1.5-μm InGaAsP amplifier having a high saturation output to optimize the material and structure parameters since the carrier lifetime dependence on the carrier density is more significant than that in the AlGaAs amplifier.

Acknowledgement. The authors wish to express their thanks to Dr. Tatsuya Kimura, Dr. Fumio Kanaya, Dr. Hiroshi Kanbe, Dr. Kenju Otsuka, and Dr. Ken-ichi Kubodera (all of Electrical Communication Labs, NTT, Musashino) for their encouragement and advice; to Dr. Akira Sugimura for his suggestions and discussions on the Auger effect, and to Dr. Yoshihisa Yamamoto (both of Electrical Communication Labs, NTT, Musashino) for his discussion on the analysis of the amplifier characteristics.

REFERENCES

1. S. Kobayashi and T. Kimura. Gain and saturation power of resonant AlGaAs laser amplifier. Electron. Lett., 16, 6, pp. 230-232 (March 1980).
2. Y. Yamamoto. Characteristics of AlGaAs Fabry-Perot cavity type laser amplifiers. IEEE J. Quantum Electron., QE-16, 10, pp. 1047-1052 (Oct. 1980).
3. T. Mukai and Y. Yamamoto. Gain, frequency bandwidth, and saturation output power of AlGaAs laser amplifiers. IEEE J. Quantum Electron., QE-17, 6, pp. 1028-1034 (June 1981).
4. J. C. Simon. Polarization characteristics of a travelling-wave-type semiconductor laser amplifier. Electron. Lett. 18, 11, pp. 438-439 (May 1982).
5. T. Nakai, R. Ito and N. Ogasawara. A symmetric frequency response of semiconductor laser amplifiers. Jpn. J. Appl. Phys., 21, 11, pp. L680-L682 (Nov. 1982).
6. T. Mukai and Y. Yamamoto. Noise in an AlGaAs semiconductor laser amplifier. IEEE J. Quantum Electron., QE-18, 4, pp. 564-575 (April 1982).
7. J. C. Simon, I. L. Favennec and J. Charil. Comparison of noise characteristics of Fabry-Perot-type and travelling-wave-type semiconductor laser amplifiers. Electron. Lett., 19, 8, pp. 288-290 (April 1983).
8. Y. Yamamoto and H. Tsuchiya. Optical receiver sensitivity improvement by a semiconductor laser preamplifier. Electron. Lett., 16, 6, pp. 233-235 (March 1980).
9. D. M. Fye. Practical limitations on optical amplifier performance. IEEE J. Lightwave Tech., LT-2, 4, pp. 403-406 (Aug. 1984).
10. G. Zeidler and D. Schicketanz. Use of laser amplifiers in a glass-fiber communications system. Siemens Forsh.-u. Entwickl.-Ber., 2, 4, pp. 227-234 (1973).
11. Y. Yamamoto. Noise and error rate performance of semiconductor laser amplifiers in a glass-fiber communications system. Siemens Forsh.-u. Entwickl.-Ber., 2, 4, pp. 227-234 (1973).
12. J. C. Simon. Semiconductor laser amplifier for single mode optical fiber communications. J. Opt. Commun., 4, 2, pp. 51-62 (June 1983).
13. T. Mukai, Y. Yamamoto and T. Kimura. S/N and error rate performance in AlGaAs semiconductor laser preamplifier and linear repeater systems. IEEE J. Quantum Electron., QE-18, 10, pp. 1560-1568 (Oct. 1982).
14. T. Mukai, T. Saitoh, O. Mikami and T. Kimura. Fabry-Perot cavity type 1.5 μm InGaAsP BH laser amplifier with small optical-mode confinement. Electron. Lett., 19, 15, pp. 582-583 (July 1983).
15. K. Takahei, H. Nagai and H. Kawaguchi. Low temperature liquid phase epitaxy growth for room-temperature cw operation of 1.55 μm InGaAsP/InP double-heterostructure laser. Appl. Phys. Lett., 36, 4, pp. 309-310 (Feb. 1980).
16. H. C. Casey, Jr. and M. B. Panish. Heterostructure Lasers, Ch. 2. Academic Press, New York (1978).
17. T. Ikegami. Reflectivity of mode at facet and oscillation mode in double-heterostructure injection lasers. IEEE J. Quantum Electron., QE-8, 6, pp. 470-476 (June 1972).
18. B. Broberg and S. Lindgren. Refractive index of $In_{1-x}Ga_xAs_yP_{1-y}$ layers and InP in transparent wavelength region. J. Appl. Phys., 55, 9, pp. 3376-3381 (May 1984).
19. H. C. Casey and F. Stern. Concentration-dependent absorption and spontaneous emission of heavily doped GaAs. J. Appl. Phys., 47, 2, pp. 631-643 (Feb. 1976).

20. F. Stern. Calculated spectral dependence of gain in excited GaAs. J. Appl. Phys., 47, 12, pp. 5382-5386 (Dec. 1976).
21. N. Dutta. Gain-current relation for $In_{0.72}Ga_{0.28}As_{0.6}P_{0.4}$ lasers. J. Appl. Phys., 52, 1, pp. 55-60 (Jan. 1981).
22. A. Sugimura. Band-to-band Auger effect in long wavelength multinary III-V alloy semiconductor lasers. IEEE J. Quantum Electron., QE-18, 3, pp. 352-363 (March 1982).
23. A. Sugimura. Band-to-band Auger recombination in InGaAsP lasers. Appl. Phys. Lett., 39, 1, pp. 21-23 (July 1981).
24. Y. Yamamoto. AM and FM quantum noise in semiconductor lasers—Part I: Theoretical analysis. IEEE J. Quantum Electron., QE-19, 1, pp. 34-46 (Jan. 1983).
25. Y. Yamamoto, S. Saito and T. Mukai. AM and FM noise in semiconductor lasers—Part II: Comparison of theoretical and experimental results for AlGaAs lasers. IEEE J. Quantum Electron., QE-19, 1, pp. 47-58 (Jan. 1983).
26. A. Yariv. Quantum Electronics, Ch. 8. John Wiley & Sons, New York (1975).
27. T. Mukai, Y. Yamamoto and T. Kimura. Optical direct amplification for fiber transmission. NTT Rev. ECL, 31, 3, pp. 340-348 (May 1983).
28. O. Mikami, H. Ando, H. Kanbe, T. Mikawa, T. Kaneda and Y. Toyama. Improved germanium avalanche photodiodes. IEEE J. Quantum Electron., QE-16, 9, pp. 1002-1007 (Sept. 1980).
29. K. Shimoda, H. Takahashi and C. H. Townes. Fluctuations in amplification of quanta with application to maser amplifiers. J. Phys. Soc. Japan, 12, 6, pp. 686-700 (June 1957).
30. Y. Yamamoto, T. Mukai and T. Kimura. Noise figure of GaAs and InGaAsP laser amplifiers. 1983 Topical Meeting on Optical Fiber Communication (OFC'83). Feb. 28-Mar. 2, New Orleans, USA, Paper, TUJ10.
31. H. A. Haus and J. A. Mullen. Quantum noise in linear amplifiers. Phys. Rev., 128, 5, pp. 2407-2413 (Dec. 1962).

APPENDIX

Table A1. Definitions of physical constants and symbols

A	Differential gain coefficient per unit time with respect to the carrier density
A_g	Differential gain coefficient per unit length with respect to carrier density
B	Bandwidth (half-width at half-maximum) of the signal gain of the Fabry-Perot cavity-type optical amplifier
B_0	Resolution bandwidth of the RF spectrum analyzer
E_g	Band-gap energy
F	Noise figure
G	Signal gain of the optical amplifier
G_e	Electrical gain of the measuring system
G_s	Single pass-gain of the optical amplifier
I	Optical intensity in the active layer
I_s	Saturation intensity
J_{nom}	Nominal current density
L	Length of the amplifier
$<M>$	Multiplication factor of the APD
N_c	Number of the injected carriers in the volume of the active layer
N_e	Density of the injected carriers
N_0	Carrier density in which the stimulated emission becomes greater than the stimulated absorption
P	Pumping rate
P_{in}	Number of injected photons in the rate equation
P_m	Noise power measured by the RF spectrum analyzer
P_{out}	Amplified signal output power
$P_{thermal}$	Thermal noise in the electrical measuring system
P_{3dB}	Saturation output power
R	Reflectivity at the facet (R_1: Input side, R_2: Output side)
R_L	Load resistance of the electrical system
V_e	Volume of the active region
V_0	Volume of the optical mode
c	Light velocity in vacuum
d	Thickness of the active layer
f	Frequency of light
f_0	Resonance frequency of the FP cavity-type optical amplifier
g	Gain coefficient (g_0 for unsaturated value)
h	Planck's constant
$<i_n^2>$	Noise power per unit load resistance

$\langle i_{ph0} \rangle$	Photocurrent corresponding to the optical output
m_e	Effective mass of electron in the conduction band
m_{hh}	Effective mass of heavy hole
m_{lh}	Effective mass of light hole
m_t	Effective transverse mode number of the spontaneous emission
m_0	Mass of free electron
n	Number of photons in the fundamental mode
n_g	Group refractive index
$\langle n_{in} \rangle$	Number of photons per second, incident on the optical amplifier
n_{sp}	Population inversion parameter ($=n_{sp1}$ and n_{ap2})
v	Ratio of the amplified signal outputs, at a resonant state and a non-resonant state
w	Width of the active layer
x	Excess-noise exponent of the APD
Γ	Optical mode confinement factor in the active layer
Δ	Energy gap of the spin orbit splitting
Δf_1	Equivalent noise bandwidth for the spontaneous emission shot noise
Δf_2	Equivalent noise bandwidth for the spontaneous-spontaneous beat noise
$\Delta\lambda_g$	Wavelength full-width which gives a positive gain coefficient
α	Absorption coefficient
β	Spontaneous emission coefficient
η	Coupling efficiency between the optical amplifier and the detector
λ	Oscillation wavelength
τ_{beat2}	Variance of the number of photons in the beat noise component
τ_{out}	Variance of the number of photons at the optical amplifier output
τ_{aug}	Carrier lifetime based on the Auger recombination
τ_{nr}	Carrier lifetime based on the non-radiative recombination
τ_p	Photon lifetime
τ_{rad}	Carrier lifetime based on the radiative recombination
τ_s	Carrier lifetime
χ	Excess noise coefficient of the optical amplifier
ω	Angular frequency in the RF region

AUTHORS (from left to right)



Takaaki Mukai graduated from Electronics Dept., Faculty of Engineering, Osaka University, in 1975; and Master's program of the same university in 1977. Since then, employed by NTT, Electrical Communication Labs., Musashino. Engaged in research into semiconductor laser and semiconductor optical amplifiers. Research Engineer of the first section, Physical Science Dept., NTT Basic Research Lab.

Tadashi Saitoh graduated from Electrical Communications Dept., Faculty of Science/Technology, Waseda University, in 1979; and Master's program of the same university in 1981. Since then, employed by NTT. Engaged in research into semiconductor laser and semiconductor optical amplifiers. Engineer in the first section, Physical Science Dept., NTT Basic Research Laboratory.

Osamu Mikami graduated from Applied Physics Dept., Faculty of Engineering, Osaka University, in 1969; and Master's program of the same university in 1971. Since then, employed by NTT Electrical Communication Labs. Engaged in research into dielectric optical recording materials, optical integrated circuits, semiconductor optics and electronic devices. Senior Research Engineer of the NTT Basic Research Lab. Dr. of Eng.